ACOUSTIC SCATTERING AND RADIATION FORCE FUNCTION EXPERIENCED BY FUNCTIONALLY GRADED CYLINDRICAL SHELLS

J. Jamali [*] **M.H. Naei** [**]

Department of Mechanical Engineering
Tehran University and Azad Shoushtar University
Tehran, Iran

F. Honarvar [**]

Department of Mechanical Engineering
K. N. Toosi University
Tehran, Iran

M. Rajabi [***]

School of Mechanical Engineering
Sharif University of Technology
Tehran, Iran

ABSTRACT

A body insonified by a sound field is known to experience a steady force that is called the acoustic radiation force. In this paper, the method of wave function expansion is adopted to study the scattering and the radiation force function caused by a plane normal harmonic acoustic wave incident upon an arbitrarily thick-walled functionally graded cylindrical shell submerged in and filled with compressible ideal fluids. A laminate approximate model and the so-called state space formulation in conjunction with the classical transfer matrix (T-matrix) approach are employed to present an analytical solution based on the two-dimensional exact equations of elasticity. Two typical models, representing the elastic properties of FGM interlayer, are considered. In both models, the mechanical properties of the graded shell are assumed to vary smoothly and continuously with the change of volume concentrations of the constituting materials across the thickness of the shell. In the first model, the simple rule of mixture governs. In the second, an elegant self-consistent micromechanical model which assumes an interconnected skeletal microstructure in the graded region is employed. Particular attention is paid on dynamical response of these models in a wide range of frequency and for different shell wall-thicknesses. In continue, by focusing on the second model, the normalized radiation force function and the form function amplitude are calculated and compared for different shell wall thicknesses and various profile of variations. Limiting cases are considered and good agreements with the solutions available in the literature are obtained.

Keywords : Sound scattering, FGM cylindrical shell, State-space method, Surface waves, Radiation force function.

1. INTRODUCTION

In recent years, the study of functionally graded materials (FGMs) has attracted a lot of attention. FGMs are a new generation of composite materials characterized by a continuously varying property due to a continuous change in the microstructural gradients (*e.g.*, composition, morphology, and crystal structure) across their thickness [1,2]. The concept of FGM was first introduced in 1984 by a group of material scientists in Japan as an alternative to laminated composite materials which show a mismatch in properties at material interfaces [3]. It takes advantage of certain desirable features of each constituent phases and optimizes the distribution of material properties such as strength, hardness, thermal resistance, *etc*., so that the desired responses to given mechanical and thermal loadings are achieved. Such materials would be useful in applications where different properties are needed at different surfaces and where reducing thermoelastic property

[*] Assistant Professor, corresponding author [**] Associate Professor [***] Graduate student

DOI : 10.1017/jmech.2011.27
Copyright © 2011 The Society of Theoretical and Applied Mechanics, R.O.C.
https://doi.org/10.1017/jmech.2011.27 Published online by Cambridge University Press

mismatch and inter-laminar stress distributions or protection of metallic or ceramic substrates against oxidation, heat penetration, wear and corrosion is critical for functionality, mechanical integrity, and lifetime improvement. In particular, FGMs have now gained widespread applicability in thermal barrier structures, blades, fusion reactors, storage tanks, and pressure vessels in form of heat, wear and corrosion resistant coatings or for joining dissimilar materials in aerospace, automobile and defense industries [3,4]. A review on various aspects of FGMs can be found in the monograph by Suresh and Mortensen [5].

The scattered pressure field from the target contains valuable information about the characteristics of the target and the surrounding medium. Appropriate exploitation of this information and proper identification of the resonance frequencies of the elastic object can serve as a powerful tool in many applications such as material characterization and non-destructive testing/evaluation of materials [6,7], remote classification of submerged targets [8,9], and on-line monitoring of elastic components [10]. The Comprehensive reviews of the sound scattering problems from cylindrical components and extensive bibliographies can be found in the works of Gaunaurd [11], Uberall [12], and Veksler [13]; here we just point out some of the recent works in this area. Honarvar and Sinclair [14] developed an exact normal-mode expansion for the scattering of a compression acoustic wave from an immersed, transversely isotropic solid cylinder. They allowed the incident acoustic wave to make an arbitrary angle with the normal to the cylindrical surface, and examined the effect of elastic constant changes on resonance frequencies of an isotropic aluminum cylinder. Hasheminejad and Rajabi [15] extended Honarvar and Sinclair's [14] analytical solution (for oblique incidence of a plane acoustic wave upon a water-submerged transversely isotropic solid cylinder) to that of a fully orthotropic cylindrical shell of arbitrary thickness based on the three-dimensional exact equations of anisotropic elasticity. They used their solutions to correlate the perturbation in the material elastic constants of an aluminium cylindrical shell to the sensitivity of resonances associated with various modes of wave propagation appearing in the backscattered amplitude spectrum (*i.e.*, axially guided, Lamb, Rayleigh and Whispering Gallery waves). Most recently, Hasheminejad and Rajabi [16] employed an exact treatment based on the inherent background coefficients to investigate the resonance scattering of time-harmonic plane acoustic waves by isotropic functionally graded cylindrical shells, at normal incidence. In this work, they just focused on the modal response of the graded shell and their primary goal was to exhibit the capability of the inherent background theories in order to isolate the modal resonance response of the structure. They used an elastic model for the FGM interlayer in which the effective structural properties can be determined from the properties and the volume concentration function of constituents, according to the rule of mixture. They showed that the resonance frequencies of the graded cylindrical components can be utilized as an indicator of the overall volume fractions and the profile of distribution of their constituents.

The resonances are the fingerprints of materials and the materials with every configuration have their own set of resonances. For NDE and on-line monitoring purposes, these resonances are used to evaluate the various properties of structures such as density, elastic constants [10,15], interfacial bonding strength [10,17] *etc*., by fitting the measured data to theoretical ones through an iterative algorithm. Therefore, appropriate exploitation of the information contained within the vibratory signals and identification of the resonance frequencies of the object can serve as a powerful tool for NDE purposes.

Resonance acoustic spectroscopy (RAS) technique is based on the resonance frequencies of the objects which are excited by insonification the submerged target with harmonic acoustic (ultrasonic) waves. While the frequency of incident waves coincides with one of the resonance frequencies of the target, the corresponding eigen-mode of the target is excited and the target starts to vibrate, emitting energy into the surrounding fluid. These vibrations of the target are then measured by sensing devices often located in far-field region of surrounding fluid medium due to destructive wave interference and fluctuating behavior of the waves in the near field zones [13]. This property, could dictate gigantic limitations in use of RAS in the cases when the surrounding fluid medium is not accessible (*e.g.*, for example, in biomedical applications such as measuring the tissue hardness or assessment of bones in osteoporosis, *etc*).

In the recent two decades, a measurable physical quantity, called the acoustic radiation force, is introduced by Lee and Wang [18]. This force is interpreted as the time-averaged force acting on an object in the sound field which is caused by a change in the energy density of the incident acoustic field [18]. The radiation force on cylindrical and spherical obstacles has recently been studied extensively due to its important applications in various technical and engineering fields such as in acoustic radiation force imaging [19], shear wave elasticity imaging [20], vibro-acoustography [21,22], and calibration of high frequency transducers [23]. The physical origin of the radiation force exerted by sound waves was probably first studied by Rayleigh [24] as a counterpart to the optical radiation force exerted by electromagnetic waves on electrically or magnetically responsive objects. The first theoretical study on cylinders goes back to the early work of Awatani [25] who developed an exact formula for the acoustic radiation force caused by progressive and stationary plane continuous-wave fields impinging on a rigid movable cylinder of variable density immersed in a compressible ideal fluid. In that study, the radiation force was numerically evaluated for a small range of size parameter values ($0 < ka < 5$). On the other hand, Zhuk [26] derived a long-wavelength approximation for the radiation force of progressive waves incident on a rigid movable cylinder. He computed the force for cylinders of variable densities immersed in non-viscous water in the range of $0 < ka < 2$. He showed that the

https://doi.org/10.1017/jmech.2011.27 Published online by Cambridge University Press

radiation force increases with increasing frequency and significantly depends on the ratio of densities of the fluid and cylinder. The theory of acoustic radiation force acting on a rigid movable cylinder in a progressive wave-field was extended by Hasegawa *et al.* [27] to include its elasticity. Further investigations were performed to study the acoustic radiation force on elastic shells in progressive waves [28]. In a series of papers, Recently Mitri modified and extended the theory of the acoustic radiation force acting on solid cylinders and cylindrical shells in progressive/ standing waves, initially developed by Hasegawa and coworkers [27,28], to the case of elastic and viscoelastic cylindrical shells [29-31].

In this paper, we employ a laminate approximate model along with the so-called state space formulation in conjunction with the transfer matrix (T-matrix) approach to develop the theory of acoustic radiation force of isotropic homogeneous cylindrical shells (*i.e.*, Mitri's work) to the orthotropic functionally graded cylindrical shells. In comparison to the rule of mixture model used by Hasheminejad and Rajabi [16], an elegant self-consistent micromechanical model which assumes an interconnected skeletal microstructure in the graded region is employed to represent the elastic properties of FGM interlayer. Particular attention is paid on comparing the dynamical response of these models in a wide range of frequency and for different shell wall-thicknesses. Also, computing the radiation force (*i.e.*, as a near-field quantity) for different profile of variation in FGM interlayer and various shell-wall thicknesses and comparing with the backscattered form function amplitude (*i.e.*, as a far-field quantity) show that how this spectrum can be used for non-contact non-destructive evaluation of design characters of FGM shells (*i.e.*, the profile of material distribution and the overall volume concentration of constituting materials). The results show that how the dips and peaks appeared in the radiation force function can be interpreted as the resonances associated with the surface waves whirling around the shell which are appeared in the scattered acoustic field.

2. FORMULATION

2.1 Basic Acoustic Field Equations

Figure 1 shows an infinite plane acoustic wave of frequency $\omega/2\pi$ incident at a submerged and fluid-filled orthotropic-FGM cylindrical shell of infinite length, inner radius a_0 and outer radius a_q. (x, y, z) is the Cartesian coordinate system with origin at o, z direction is coincident with the axis of the cylindrical shell, and (r, θ, z) is the corresponding cylindrical polar coordinate system. The field equations for an inviscid and ideal compressible medium that can not support shear stresses may conveniently be expressed in terms of a scalar velocity potential as [32]

$$\mathbf{v} = -\nabla\varphi\ , \quad p = -i\,\omega\,\rho\,\varphi\ , \quad \nabla^2\varphi + k^2\varphi = 0\ , \qquad (1)$$

where $k = \omega/c$ is the wave number for the dilatational wave, c is the speed of sound, ρ is the ambient density, $\mathbf{v}$ is the fluid particle velocity vector, and p is the acoustic pressure.

The dynamics of the problem may be expressed in terms of appropriate scalar potentials that can be represented in the form of an infinite generalized Fourier series whose unknown scattering coefficients are to be determined by imposing the proper boundary conditions. The expansion of the incident plane wave, propagating in the surrounding fluid medium, in cylindrical coordinate (see Fig. 1) has the form [32]

$$\varphi_{inc.}(r,\ \theta,\ \omega) = \varphi_0 \sum_{n=0}^{\infty} \varepsilon_n\, i^n J_n(k_1 r)\cos(n\,\theta)\, e^{-i\omega t}\ , \qquad (2)$$

where $k_1 = \omega/c_1$ is the wave number in the outer fluid medium 1 (see Fig. 1), J_n is the cylindrical Bessel function of the first kind of order n, symbol ε_n is the Neumann factor ($\varepsilon_n = 1$ for $n = 0$, and $\varepsilon_n = 2$ for $n > 0$), $i = \sqrt{-1}$, and φ_0 is the amplitude of the incident wave. Likewise, keeping in mind the radiation condition, the solutions of the Helmholtz equation for the scattered potential in the surrounding fluid medium 1, and the transmitted potential in the inner fluid medium 2 can be expressed as a linear combination of cylindrical waves as [32]

$$\varphi_1(r,\ \theta,\ \omega) = \sum_{n=0}^{\infty} \varepsilon_n\, i^n A_n(\omega) H_n^{(1)}(k_1 r)\cos(n\theta)\ e^{-i\omega t}\ ,$$

$$\varphi_2(r,\ \theta,\ \omega) = \sum_{n=0}^{\infty} \varepsilon_n\, i^n B_n(\omega) J_n(k_2 r)\ \cos(n\theta)\, e^{-i\omega t}\ , \qquad (3)$$

where $k_2 = \omega/c_2$ is the acoustic wave number in the inner medium 2, $H_n^{(1)}(x) = J_n(x) + i\,Y_n(x)$ is the cylindrical Hankel function of the first kind of order n, $Y_n(x)$ is the cylindrical Bessel function of the second kind of order n, A_n and B_n are unknown scattering and transmission coefficients. Furthermore, using (1), the acoustic pressures and radial velocities in the fluid mediums 1 and 2 are respectively written as

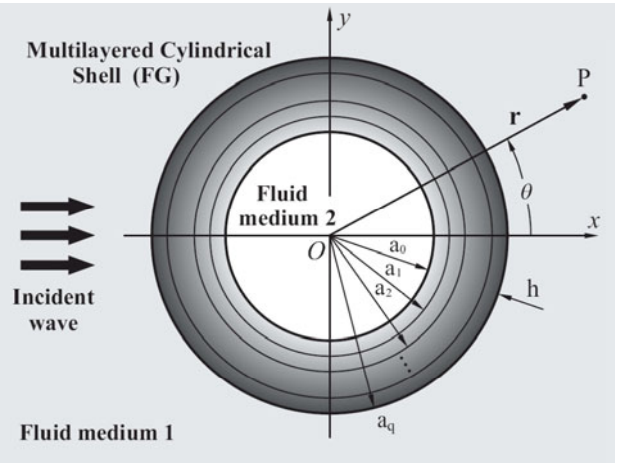


Fig. 1 Problem geometry

https://doi.org/10.1017/jmech.2011.27 Published online by Cambridge University Press

$$p_1 = -i\omega\rho_1(\varphi_{inc.} + \varphi_1)$$
$$= -\omega\rho_1 \sum_{n=0}^{\infty} i^{n+1}\varepsilon_n \left[\varphi_0 J_n(k_1 r) + H_n^{(1)}(k_1 r) A_n(\omega)\right] \cos(n\theta) e^{-i\omega t} ,$$

$$p_2 = -i\omega\rho_2 \varphi_2$$
$$= -\sum_{n=0}^{\infty} \omega\rho_2 \varepsilon_n i^{n+1} J_n(k_2 r) B_n(\omega) \cos(n\theta) e^{-i\omega t} , \quad (4)$$

and

$$v_r^{(1)} = -\frac{\partial(\varphi_{inc.} + \varphi_1)}{\partial r}$$
$$= -k_1 \sum_{n=0}^{\infty} \varepsilon_n i^n \left[\varphi_0 J_n'(k_1 r) + H_n^{(1)\prime}(k_1 r) A_n(\omega)\right] \cos(n\theta) e^{-i\omega t} ,$$
$$v_r^{(2)} = -\frac{\partial\varphi_2}{\partial r} = -k_2 \sum_{n=0}^{\infty} \varepsilon_n i^n J_n'(k_2 r) B_n(\omega) \cos(n\theta) e^{-i\omega t} . \quad (5)$$

where prime denotes differentiation with respect to the argument.

2.2 Sandwich Cylindrical Shell

Now, we consider a sandwich cylindrical shell of uniform thickness h, with a functionally graded interlayer core of uniform thickness h_I, inner radius a_0 and outer radius a_q with variable material properties suspended in and filled with ideal compressible fluid mediums. Adopting a laminate model [16,33,34], the sandwich cylindrical shell is assumed to be composed of q sublayers of homogeneous orthotropic materials which are perfectly bonded at their interfaces and lined up such that their axes of symmetry coincide with each other (Fig. 1). The solution is expected to gradually approach the exact one as the number of sublayers (the thickness of sublayers) increases (decreases). The material properties within each layer of inner radius a_{k-1}, outer radius a_k and uniform thickness $h_k = a_k - a_{k-1}$, are described by the elastic coefficients c_{ij}^k and mass density ρ_c^k where $k = 1, \ldots, q$. In continue, we are looking for a technique to solve the equations of motion for k-th layer of multilayered cylindrical shell.

2.2.1 Local Transfer Matrix

Now, consider a cylindrically orthotropic hollow cylinder of infinite length, inner radius a_{k-1}, outer radius a_k and uniform thickness $h_k = a_k - a_{k-1}$. In a linearly elastic continuum, the equations of motion, in the absence of body forces, in terms of the stress components are written as [35]

$$\frac{\partial\sigma_{rr}^k}{\partial r} + \frac{\partial\sigma_{r\theta}^k}{r\partial\theta} + \frac{1}{r}(\sigma_{rr}^k - \sigma_{\theta\theta}^k) = \rho_c^k \frac{\partial^2 u_r^k}{\partial t^2} ,$$
$$\frac{\partial\sigma_{r\theta}^k}{\partial r} + \frac{\partial\sigma_{\theta\theta}^k}{r\partial\theta} + \frac{2}{r}\sigma_{r\theta}^k = \rho_c^k \frac{\partial^2 u_\theta^k}{\partial t^2} , \quad (6)$$

where ρ_c^k is the solid material density, and u_r^k, u_θ^k are the material displacements in the r and θ directions, respectively. Also, the Hooke's law in the polar coordinate system may be written as [36]

$$\sigma_{rr}^k = c_{11}^k \varepsilon_{rr}^k + c_{12}^k \varepsilon_{\theta\theta}^k , \quad \sigma_{\theta\theta}^k = c_{12}^k \varepsilon_{rr}^k + c_{22}^k \varepsilon_{\theta\theta}^k , \quad \sigma_{r\theta}^k = c_{33}^k \varepsilon_{r\theta}^k , \quad (7)$$

where

$$\varepsilon_{rr}^k = \frac{\partial u_r^k}{\partial r} , \quad \varepsilon_{\theta\theta}^k = \frac{\partial u_\theta^k}{r\partial\theta} + \frac{u_r^k}{r} , \quad \varepsilon_{r\theta}^k = \frac{\partial u_r^k}{r\partial\theta} + \frac{\partial u_\theta^k}{\partial r} - \frac{u_\theta^k}{r} . \quad (8)$$

where c_{ij}^k are the elastic constants in polar coordinate system.

Now, following the state space approach [16,37,38], the state equations can be derived by direct substitution of the constitutive relation (7) and compatibility relation (8) into the equations of motion (6), which after some manipulations, leads to:

$$\frac{\partial\mathbf{Y}^k}{\partial r} = \mathbf{M}^k \mathbf{Y}^k , \quad (9)$$

where $\mathbf{Y}^k = [u_\theta^k, u_r^k, \sigma_{rr}^k, \sigma_{r\theta}^k]^T$ is the state vector, and $\mathbf{M}^k$ is a 4 × 4 coefficient matrix whose elements are provided in Appendix I. Next, by employing the appropriate normal mode expansions [15,39], the state vector $\mathbf{Y}^k$ is expanded in terms of unknown modal coefficients as

$$\mathbf{Y}^k = \begin{Bmatrix} u_\theta^k \\ u_r^k \\ \sigma_{rr}^k \\ \sigma_{r\theta}^k \end{Bmatrix} = \sum_{n=0}^{\infty} \begin{Bmatrix} a_q u_{\theta,n}^k(\xi) \sin(n\theta) \\ a_q u_{r,n}^k(\xi) \cos(n\theta) \\ c_{33}^q \sigma_{rr,n}^k(\xi) \cos(n\theta) \\ c_{33}^q \sigma_{r\theta,n}^k(\xi) \sin(n\theta) \end{Bmatrix} e^{-i\omega t} , \quad (10)$$

where $\xi = r/a_q$ is the dimensionless radial coordinate, c_{33}^q is one of the elements of stiffness matrix of q-th layer (outer layer) of multilayered shell and the subscript ". , n" denotes the n'th circumferential mode number. Subsequent substitution of (10) into (9), and utilizing the orthogonality of trigonometric functions, we obtain

$$\frac{d\mathbf{V}_n^k}{d\xi} = \mathbf{D}_n^k(\xi)\mathbf{V}_n^k , \quad (11)$$

where $\mathbf{V}_n^k = [u_{\theta,n}^k, u_{r,n}^k, \sigma_{rr,n}^k, \sigma_{r\theta,n}^k]^T$ is the modal state vector, and $\mathbf{D}_n^k(\xi)$ is a 4 × 4 modal coefficient matrix whose elements are given in Appendix II.

In the literature, two different classes of techniques can be found for solving the coupled system of first-order ordinary differential Eq. (11). In the first group, the solution is directly sought after, which makes this approach quite intricate and computationally intensive [40,41]. In the second class, which is also used in this paper, a laminate approximate model is adopted which the details could be found in Refs. [16,37,38,42]; As

https://doi.org/10.1017/jmech.2011.27 Published online by Cambridge University Press

the thickness of each sublayer is supposed to be very small, the coefficient matrix $\mathbf{D}_n^k$ can advantageously be assumed constant within each sublayer, which we denote as $\mathbf{D}_n^k(\xi_{k-1})$ for the k-th sublayer, where $\xi_{k-1} = a_{k-1}/a_q$. Thus, within the k-th sublayer, the solution to Eq. (11) can be written as

$$\mathbf{V}_n^k(\xi) = \mathbf{V}_n^k(\xi_{k-1}) \exp\left[(\xi - \xi_{k-1})\mathbf{D}_n^k(\xi_{k-1})\right], \qquad (12)$$

where $\xi_{k-1} \le \xi \le \xi_k$, and $k = 1, \ldots, q$. Subsequent evaluation of Eq. (12) at the outer surface of the k-th sublayer, leads to the following useful recurrence relation:

$$\mathbf{V}_n^k(\xi_k) = \mathbf{L}_n^k \mathbf{V}_n^k(\xi_{k-1}), \qquad (13)$$

where $\mathbf{L}_n^k = \exp\left[h_k \mathbf{D}_n^k(\xi_{k-1})/a_q\right]$ is a 4 × 4 local transfer matrix corresponding to k-th layer of multilayered cylindrical shell which relates the state variables at the outer surface of the k-th sublayer to those at the inner surface.

2.2.2 Global Transfer Matrix and Boundary Conditions

Finally, by invoking the continuity conditions between all interface layers, the state variables at outer radius of the cylindrical shell (*i.e.*, at $r = a_q$ for which $\xi_q = 1$) are advantageously related to those at inner radius (*i.e.*, at $r = a_0$ for which $\xi_0 = a_0/a_q$) by

$$\mathbf{V}_n^q(\xi_q) = \mathbf{T}_n \mathbf{V}_n^1(\xi_0), \qquad (14)$$

where $\mathbf{T}_n = \prod_{k=1}^{q} \mathbf{L}_n^k = \prod_{k=1}^{q} \exp\left[h_k \mathbf{D}_n^k(\xi_{k-1})/a_q\right]$ is the 4 × 4 global modal transfer matrix [43] corresponding to the multilayered cylindrical shell.

The unknown coefficients A_n and B_n and the elements of the modal state variable vector, $\mathbf{V}_n^1(\xi_0) = [u_{\theta,n}^0, u_{r,n}^0, \sigma_{rr,n}^0, \sigma_{r\theta,n}^0]^T$ can be determined from the appropriate boundary conditions imposed at the inner ($r = a_0$) and the outer ($r = a_q$) surfaces of the multilayered shell. Thus, assuming continuity of normal fluid and solid velocities, normal stress and fluid pressure, and vanishing of tangential stress at $r = a_0$ and $r = a_q$ imply that

$$\begin{aligned}
&(-i\omega)\, u_r(r, \theta, \omega)\big|_{r=a_0,a_q} = v_r(r, \theta, \omega)\big|_{r=a_0,a_q}, \\
&\sigma_{rr}(r, \theta, \omega)\big|_{r=a_0,a_q} = -p(r, \theta, \omega)\big|_{r=a_0,a_q}, \\
&\sigma_{r\theta}(r, \theta, \omega)\big|_{r=a_0,a_q} = 0,
\end{aligned} \qquad (15)$$

Finally, making use of (4) and (14) in (15), we obtain the following 6 × 6 coupled linear system of equations

$$\begin{bmatrix}
C_{1,n} & 0 & T_n^{2,1} & T_n^{2,2} & T_n^{2,3} & T_n^{2,4} \\
0 & C_{2,n} & 0 & 1 & 0 & 0 \\
C_{3,n} & 0 & T_n^{3,1} & T_n^{3,2} & T_n^{3,3} & T_n^{3,4} \\
0 & C_{4,n} & 0 & 0 & 1 & 0 \\
0 & 0 & 0 & 0 & 0 & 1 \\
0 & 0 & T_n^{4,1} & T_n^{4,1} & T_n^{4,1} & T_n^{4,1}
\end{bmatrix}
\begin{Bmatrix}
A_n \\ B_n \\ u_{\theta,n}^0 \\ u_{r,n}^0 \\ \sigma_{rr,n}^0 \\ \sigma_{r\theta,n}^0
\end{Bmatrix} =
\begin{bmatrix}
C_{5,n} \\ 0 \\ C_{6,n} \\ 0 \\ 0 \\ 0
\end{bmatrix}, \qquad (16)$$

where $T_n^{i,j}$ ($i,j = 1, 2, \ldots, 4$) are elements of the global modal transfer matrix, $\mathbf{T}_n$, and

$$\begin{aligned}
C_{1,n} &= -k_1 \varepsilon_n i^{n-1} H_n^{(1)\prime}(k_1 a_q)/\omega a_q, \\
C_{2,n} &= -k_2 \varepsilon_n i^{n-1} J_n'(k_2 a_0)/\omega a_q, \\
C_{3,n} &= -\omega\rho_1 \varepsilon_n i^{n+1} H_n^{(1)}(k_1 a_q)/c_{33}^q, \\
C_{4,n} &= \omega\rho_2 \varepsilon_n i^{n+1} J_n(k_2 a_0)/c_{33}^q, \\
C_{5,n} &= \varphi_0 k_1 \varepsilon_n i^{n-1} J_n'(k_1 a_q)/\omega a_q, \\
C_{6,n} &= \omega\rho_1 \varphi_0 \varepsilon_n i^{n+1} J_n(k_1 a_q)/c_{33}^q.
\end{aligned} \qquad (17)$$

2.3 Functionally Graded Model

2.3.1 Model I

The first model is as same as the model used by Hasheminejad and Rajabi [16] in which the rule of mixture governs on the Lame constants and the material density function of graded shell. Considering the aforementioned laminate model of the cylindrical shell, we have

$$\begin{aligned}
\lambda^k &= V_F(\bar{r}_k)\lambda^1 + \left[1 - V_F(\bar{r}_k)\right]\lambda^q, \\
\mu^k &= V_F(\bar{r}_k)\mu^1 + \left[1 - V_F(\bar{r}_k)\right]\mu^q, \\
\rho^k &= V_F(\bar{r}_k)\rho^1 + \left[1 - V_F(\bar{r}_k)\right]\rho^q,
\end{aligned} \qquad (18)$$

where $\bar{r}_k = (a_{k-1} + a_k)/2$ ($k = 1, 2, \ldots, q$) and $V_F(\bar{r}_k)$ is the volume fraction of constituting materials in the k-th sublayer. Also, the elastic constants of the sublayeres can be expressed in terms of these Lame constants as

$$\begin{aligned}
c_{11}^k &= c_{22}^k = c_{33}^k = \lambda^k + 2\mu^k, \\
c_{12}^k &= c_{13}^k = c_{23}^k = \lambda^k, \\
c_{44}^k &= c_{55}^k = c_{66}^k = \mu^k.
\end{aligned} \qquad (19)$$

2.3.2 Model II

In this model, an elegant self-consistent micromechanical model [44,45] which assumes an interconnected skeletal microstructure in the graded region is employed. According to this model, no distinctions between the constituent phases are made and the same overall moduli are predicted in another composite in which the roles of the phases are interchanged. Consequently, the locally effective bulk modulus of the FGM interlayer may be related to the elastic moduli of the constituent materials as

$$K^k = \left[\frac{1 - V_F^k(\bar{r}_k)}{K^q + 4\mu^k/3} + \frac{V_F^k(\bar{r}_k)}{K^1 + 4\mu^k/3}\right]^{-1} - \frac{4\mu^k}{3}, \qquad (20)$$

where $\bar{r}_k = (a_{k-1} + a_k)/2$ ($k = 1, 2, \ldots, q$) and $V_F(\bar{r}_k)$ is the volume fraction of constituting materials in the k-th sublayer. Also μ^k (effective shear modulus of the k-th layer) is obtained by solving the following quartic equation:

https://doi.org/10.1017/jmech.2011.27 Published online by Cambridge University Press

$$\frac{\left[1-V_F^k(\bar{r}_k)\right]K^q}{K^q+4\mu^k/3}+\frac{V_F^k(\bar{r}_k)K^1}{K^1+4\mu^k/3}+$$
$$5\left\{\frac{\left[1-V_F^k(\bar{r}_k)\right]\mu^1}{\mu^k-\mu^1}+\frac{V_F^k(\bar{r}_k)\mu^q}{\mu^k-\mu^q}\right\}+2=0\ , \qquad (21)$$

Also, assuming that the density ratio contrast between constituents is not too high, it is appropriate to assume that the effective density of the FGM interlayer is the mean density, given by the straightforward rule-of-mixtures as

$$\rho^k=V_F(\bar{r}_k)\rho^1+\left[1-V_F(\bar{r}_k)\right]\rho^q\ , \qquad (22)$$

and the elastic constants of the sublayeres can be expressed as

$$\begin{aligned} c_{11}^k&=c_{22}^k=c_{33}^k=K^k+4\mu^k/3\ ,\\ c_{12}^k&=c_{13}^k=c_{23}^k=K^k-2\mu^k/3\ ,\\ c_{44}^k&=c_{55}^k=c_{66}^k=\mu^k\ . \end{aligned} \qquad (23)$$

2.4 The Scattering Form Function Amplitude and the Averaged Radiation Force

The most relevant acoustic field quantity is the scattering form function. The standard definition of the (far-field) form function amplitude is given by [12,13,46]

$$|f_\infty(\theta=\pi,\ \omega)|\approx \lim_{r\to\infty}\sqrt{\frac{2r}{\mathrm{a_q}}}\left|\frac{\varphi_1(r,\theta=\pi,\omega)}{\varphi_{inc}}\right|$$
$$=\left|\sum_{n=0}^{\infty}f_n(\theta=\pi,k_1\mathrm{a}_q)\right|\ , \qquad (24)$$

where

$$f_n(\theta,\ K_1\,\mathrm{a}_q)=\frac{2\varepsilon_n}{\sqrt{\pi i\,k_1\,\mathrm{a}_q}}A_n\cos(n\theta)\ , \qquad (25)$$

is referred to as the global scattering coefficient for n-th mode. Another quantity of interest is average radiation force acting on the target. The acoustic radiation force is caused by a transfer of momentum from the wave to the medium, arising either from absorption or reflection of the wave in or at the second medium (target). The magnitude of this force is dependent upon both the medium properties and the acoustic beam parameters. Acoustic radiation force is commonly interpreted as the time-averaged force which, under the conditions at which it is measured, depends on the difference in the energy densities on the two sides of the target. It can thus be calculated by integrating the momentum flux tensor over the target surface and over time. The general theory of the acoustic radiation force on a boundary moving with a velocity of the first order was first developed by Yosioka and Kawasima [47] and is expressed in vector form as

$$\langle\mathbf{F}\rangle=-\int\!\!\int_S\left[\left(\frac{1}{2}\frac{\rho_1}{c_1^2}\left\langle(\partial\varphi/\partial t)^2\right\rangle-\frac{1}{2}\rho_1\left\langle\left(|\nabla\varphi|^2\right)\right\rangle\right)\mathbf{e}_r\right.$$
$$\left.+\rho_1\left\langle(v_r\,\mathbf{e}_r+v_\theta\,\mathbf{e}_\theta)v_r\right\rangle\right]\mathrm{d}S \qquad (26)$$

where $\boldsymbol{S}$ is the target's surface at its equilibrium position, $\varphi=\varphi_{inc.}+\varphi_1$ is the total velocity potential in the surrounding fluid medium, the symbol $\langle.\rangle$ denotes the time averaging, and $v_r=-\partial\varphi/\partial r$ and $v_\theta=-\partial\varphi/r\partial\theta$ are the radial and tangential components of the fluid particle velocity at the target's boundary, respectively. After proper substitutions and with some relatively lengthy manipulations, the final expression of the radiation force for an incident plane progressive wave in the direction of wave propagation can greatly be simplified and is given by [28,30]

$$\langle F_x\rangle=Y_p\,S_c\langle E_p\rangle \qquad (27)$$

where $\langle E_p\rangle=(1/2)\,\rho_1\,k_1^2\,|\,\varphi_0\,|^2$ is the mean energy density of the incident wave, $S_c=2\mathrm{a}_q$ is the cross-sectional area of scatterer (FGM shell), and Y_p is a dimensionless factor called the radiation force function (radiation force per unit cross-section and unit energy) which can be expressed as [28,30]

$$Y_p(k_1\,\mathrm{a}_q)=-\frac{2}{(k_1\,\mathrm{a}_q)}\sum_{n=0}^{\infty}\left[\alpha_n+\alpha_{n+1}+2(\alpha_n\,\alpha_{n+1}+\beta_n\,\beta_{n+1})\right] \qquad (28)$$

in which the coefficients α_n and β_n are the real and imaginary parts of the scattering coefficient A_n, respectively.

3. NUMERICAL RESULTS

In order to illustrate the nature and general behavior of the solution, we consider some numerical examples. Realizing the large number of parameters involved here while keeping in view our computing hardware limitations, we confine our attention to a particular problem. The surrounding and filling fluids are respectively assumed to be water ($\rho_1=1000$ kg/m^3, $c_1=1480$ m/s) and air ($\rho_2=1.2$ kg/m^3, $c_2=344$ m/s) at atmospheric pressure and ambient temperature.

The cylindrical shell is assumed to be three-layered in which the interlayer (thickness $h_I=h_{i+1}+h_{i+2}+\ldots+h_{j-1}+h_j$, $i>0$ and $j<q$) is graded in the radial direction with varying proportions of metallic aluminium (Al) substrate (thickness $h_a=h_1+\ldots+h_i$,) and ceramic zirconia (ZrO_2) coating (thickness $h_b=h_{j+1}+h_{j+2}+\ldots+h_q$). The volume fraction of metal in the FGM interlayer is varied from 100% on the inner interface (at $r=\mathrm{a}_0+h_a=\mathrm{a}_i$) to zero on the outer interface (at $r=\mathrm{a}_0+h_a+h_I=\mathrm{a}_j$). A typical variation in volume fraction of Al along the radial axis is shown in Fig. 2. In this work, the gradient profiles for the functionally graded interphase is called the power-law distribution in which the volume fraction of Al in $\mathrm{a}_i\le r\le\mathrm{a}_j$, is assumed as follows

https://doi.org/10.1017/jmech.2011.27 Published online by Cambridge University Press

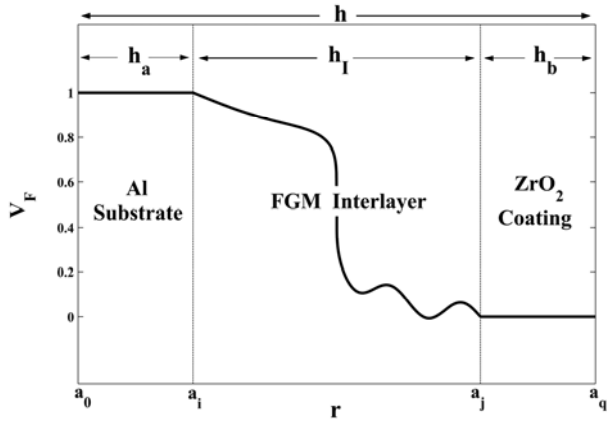


Fig. 2 Variations in volume fraction of aluminum in a general composition of sandwich shell with FGM interlayer

$$V_F(r) = \left(1 - \frac{r - a_i}{h_I}\right)^{\gamma} , \tag{29}$$

Also, the overall volume concentration of Al (inner constituent) may be calculated as written in follow

$$\overline{V}_F = \frac{\int_{a_0}^{a_q} V_F(r)\, r\, dr}{\int_{a_0}^{a_q} r\, dr} . \tag{30}$$

A MATLAB code was constructed for computing the global transfer matrix, $\mathbf{T}_n$, treating boundary conditions and to calculate the unknown scattering coefficients, and the global and the inherent background coefficients as functions of the nondimensional frequency $k_1 a_q$ for a unit amplitude incident plane wave ($\varphi_0 = 1$). The computations were performed on a Pentium IV personal computer with a maximum number of layers $q_{max} = 100$, a maximum truncation constant of $n_{max} = (k_1 a_q)_{max} + 15$, especially selected to assure convergence in case of a thick FGM interlayer and also in the high frequency range. The convergence was systematically checked in a simple trial and error manner, by increasing the number of layers, q, as well as the truncation constant (*i.e.*, by including more modes in all summations) while looking for steadiness or stability in the numerical value of the solutions.

In the research work made by Hasheminejad and Rajabi [16], the effect of relative thickness of FGM mid-layer (*i.e.*, h_I / h) on the resonant response of the structure has been studied where the total thickness of the shell is assumed to be constant (*i.e.*, $h / a_q = 0.1$). Since, here we just focus on the case that the Al substrate and the ZrO_2 coating are absent (*i.e.*, we have a single layer functionally graded cylindrical shell; $h_a = h_b = 0$, $h_I / h = 1$). The material properties are shown in Table 1.

Figures 3(a) and 3(b) compare the frequency response of model I (*i.e.*, dotted-line) and model II (*i.e.*, solid-line), by exhibiting the variations of the backscattering form function amplitude, $|f(\theta = \pi, k_1 a_q)|$, with dimensionless frequency, $k_1 a_q$, for a functionally graded

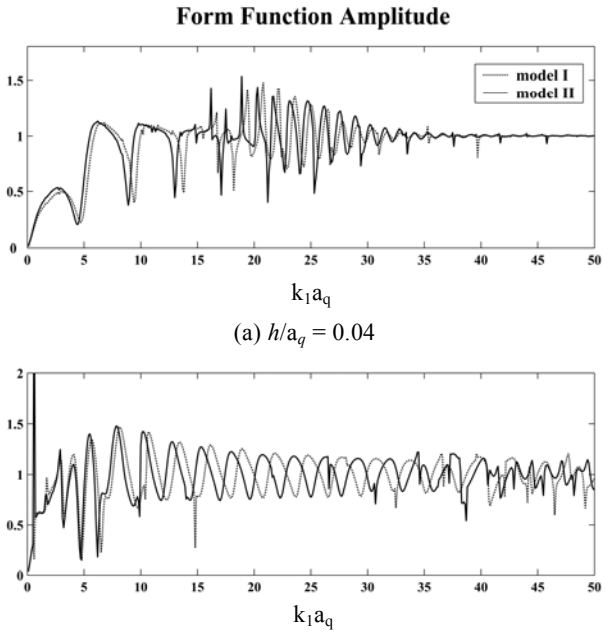


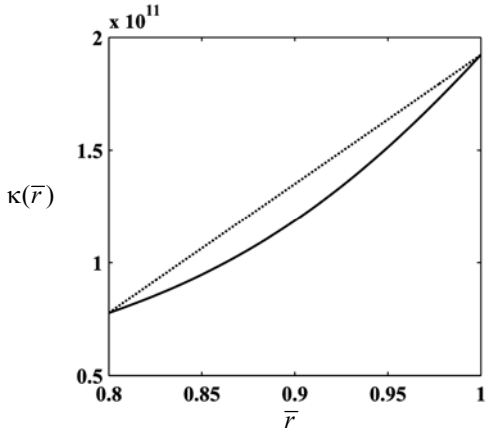
Fig. 3 Variations of backscattering form function amplitudes with selected thicknesses ((a): h/a_q = 0.04, (b): h/a_q = 0.2) for a functionally graded cylindrical shell with linear profile of variation (*i.e.*, $\gamma = 1$).
(····· model I; ——— model II)

Table 1 Material properties

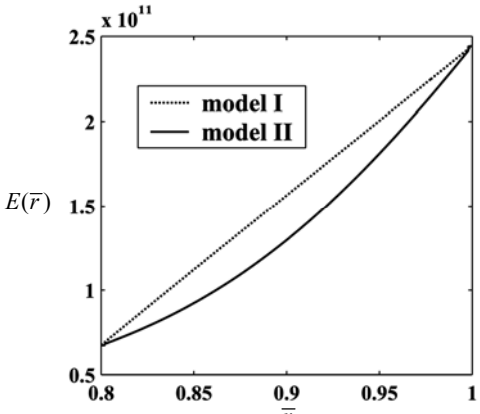
Material	ρ_s (kg/m^3)	c_{11}, c_{22}, c_{33} (GPa)	c_{44}, c_{55}, c_{66} (GPa)	c_{12}, c_{13}, c_{23} (GPa)
Aluminium (Al)	2706	110.47	26.69	57.09
Zirconia (ZrO_2)	5700	318.60	94.80	129.00

cylindrical thin shell of thickness $h / a_q = 0.04$ and a relatively thick functionally graded cylindrical shell of thickness $h / a_q = 0.2$. A linear distribution of constituting materials according to the power-law variation (*i.e.*, $\gamma = 1$) has been considered. Figures 4(a) ~ 4(f) compare the variation of the elastic properties (*i.e.*, E, ν, λ, μ, κ) and mass density (*i.e.*, ρ) along the radial axis (*i.e.*, diemnsionless radial coordinate: $\overline{r} = r / a_q$), for model I and II. As Fig. 3 shows, the dips and peaks (*i.e.*, resonances) associated to the response of model II have a left-ward shift in comparison to those associated to the model I, especially for higher frequencies. Considering Figs. 4(a) ~ 4(d), this behavior may be interpreted in this way that the model I supplies the higher overall stiffness for the graded shell in comparison to the model II. Also, the observed differences are more pronounced in the case of thick shell of $h / a_q = 0.2$ thickness which indicates the outstanding role of the elasticity properties for higher thicknesses of the shell.

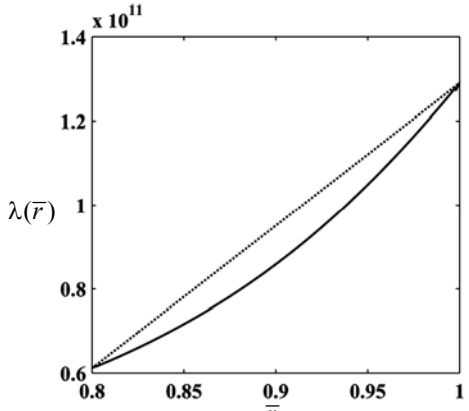
https://doi.org/10.1017/jmech.2011.27 Published online by Cambridge University Press



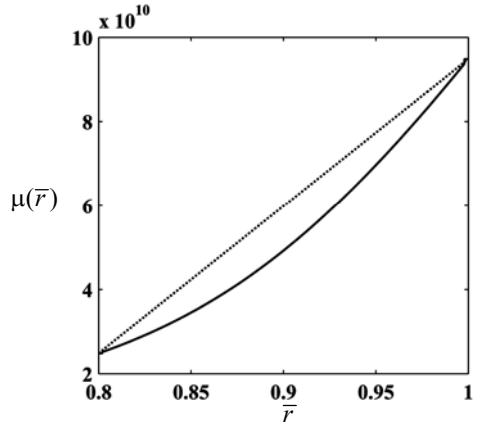
(a) $\kappa(\bar{r})$



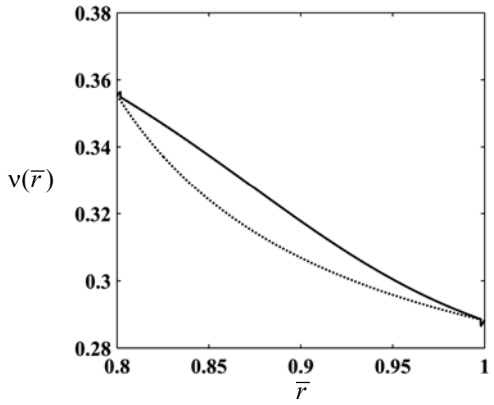
(b) $E(\bar{r})$



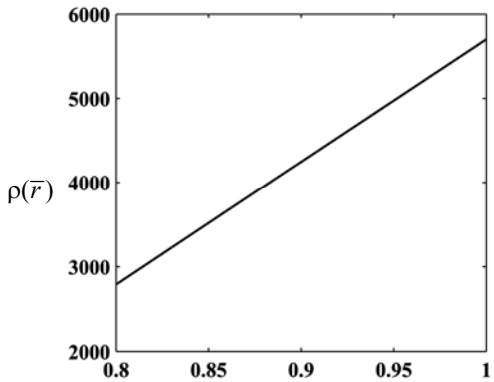
(c) $\lambda(\bar{r})$



(d) $\mu(\bar{r})$



(e) $\nu(\bar{r})$



(e) $\rho(\bar{r})$

Fig. 4 Variations of elasticity properties with normalized radial coordinate ((a): $\kappa(\bar{r})$ (b): $E(\bar{r})$, (c): $\lambda(\bar{r})$, (d): $\mu(\bar{r})$, (e): $\nu(\bar{r})$, (f) $\rho(\bar{r})$) for a thick (h/a_q = 0.2) functionally graded hollow cylinder with linear profile of variation (*i.e.*, $\gamma = 1$)
(····· model I; ——— model II)

What follows, we study the variations of the normalized radiation force function (*i.e.*, Y_p) and the back-scattered form function (*i.e.*, $|f_\infty|$) amplitudes with normalized frequency, $k_1 a_q$, for different profile of distribution in which the overall volume concentration of Al vary linearly from zero (*i.e.*, single ZrO_2 shell) to one (*i.e.*, single Al shell) and for different shell wall-thicknesses. Using a root-finder code, the γ constant in Eq. (29) is found so that the discrete values corresponding to the overall volume concentration of Al be obtained. Table 2 contains the obtained γ constants corresponding to the discrete values of $\bar{V}_F$ = [0.1, 0.3, 0.5, 0.7, 0.9] for different shell thicknesses, h/a_q = [0.04, 0.1, 0.5, 0.9]. Figure 5 shows the variation of the volume fraction profiles with dimensionless radial coordinate, $\bar{r}$, associated to discrete values of overall volume concentration of Al (*i.e.*, $\bar{V}_F$ = 0.1, 0.3, 0.5, 0.7, 0.9), for graded shell with h/a_q = 0.04 thickness. Due to the general similarity between the volume fraction profiles for h/a_q = 0.04 shell and other shell-wall thicknesses (*i.e.*, h/a_q = 0.1, 0.5, 0.9) and in order to

https://doi.org/10.1017/jmech.2011.27 Published online by Cambridge University Press

Table 2 Index values, γ, corresponding to the discrete values of overall volume fraction, $\bar{V}_F$, for selected shell wall thicknesses

	$\bar{V}_F = 0.9$	$\bar{V}_F = 0.7$	$\bar{V}_F = 0.5$	$\bar{V}_F = 0.3$	$\bar{V}_F = 0.1$
$h/a_q = 0.04$	γ = 0.11	γ = 0.43	γ = 1	γ = 2.35	γ = 8.93
$h/a_q = 0.1$	γ = 0.10	γ = 0.42	γ = 0.98	γ = 2.25	γ = 8.67
$h/a_q = 0.5$	γ = 0.09	γ = 0.36	γ = 0.81	γ = 1.81	γ = 6.51
$h/a_q = 0.9$	γ = 0.07	γ = 0.28	γ = 0.61	γ = 1.25	γ = 3.66

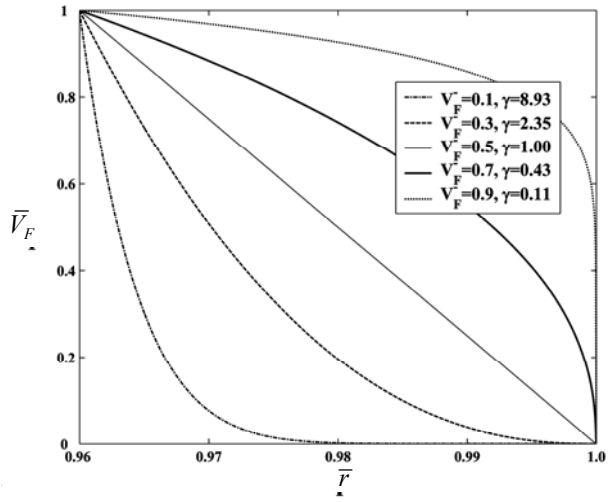
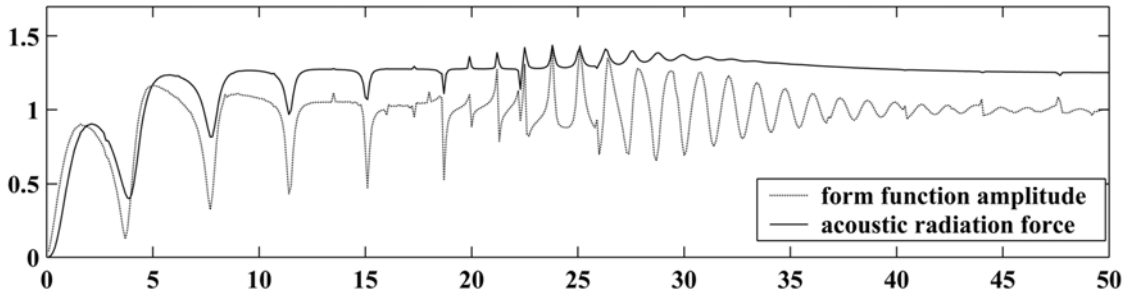


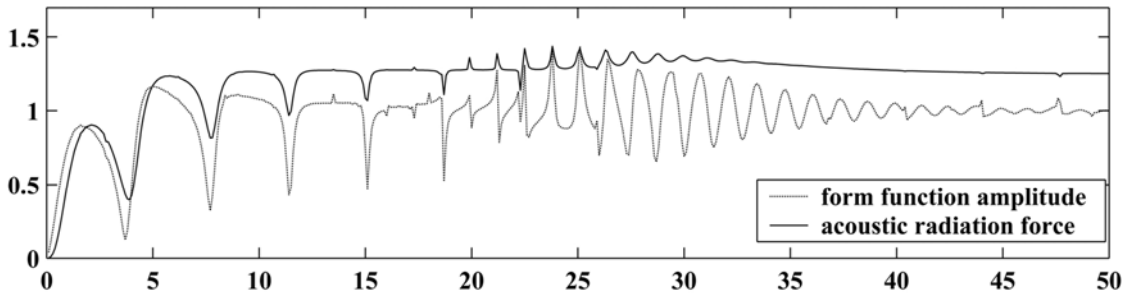
Fig. 5 Variations in volume fraction of aluminum in FGM interlayer of a h/a_q = 0.04 thickness functionally graded cylindrical shell (— — · γ = 2.35, —— γ = 1, —— γ = 0.43, ... γ = 0.11, – · – γ = 8.93)

avoid lengthening the manuscript, we do not plot them. Also, Figs. 6 ~ 9 exhibit the variations of the normalized radiation force function, Y_p (*i.e.*, solid-line) and the normalized backscattering form function amplitudes, $|f_\infty(\theta = \pi)|$ (*i.e.*, dotted-line) with dimensionless frequency, $k_1 a_q$, for distinct values of overall volume fractions of constituents, $\bar{V}_F$ = [0.1, 0.3, 0.5, 0.7, 0.9], associated to different shell wall-thicknesses h / a_q = 0.04, 0.1, 0.5 and 0.9, respectively. The most important observations are as follows.

It is well-known that the form function amplitude consists of a smooth background and the resonance spectra. The background signal or the non-resonant part of scattered acoustic field is due to the overall rigidity of the shell. Many of dips and peaks appeared in the form function amplitude spectra correspond to the resonance modes of the shell which are originated from the standing surface waves formed around the cylindrical shell. As Figs. 6 ~ 9 exhibit, for different thicknesses of the graded shell and different profiles of distribution, the maxima and minima appeared in the radiation force function are in consistent with the dips and peaks projected in the form function spectra. This phenomenon proves that the radiation force function can be used as an indicator of the resonance frequencies of the (FGM) cylindrical shells. This compatibility is more visible especially in the case of thin shells which the resonances have a sharp pattern (*i.e.*, low damping). Also, some of the resonances manifest themselves as either minima or maxima which this phenomenon may be linked to the phase difference between the traveling surface waves around the shell and the scattered bulk waves. Hence, when the scattered bulk waves and the surface waves are out of phase, resonance peaks appear as minima instead of maxima in the total scattering cross-section curves.

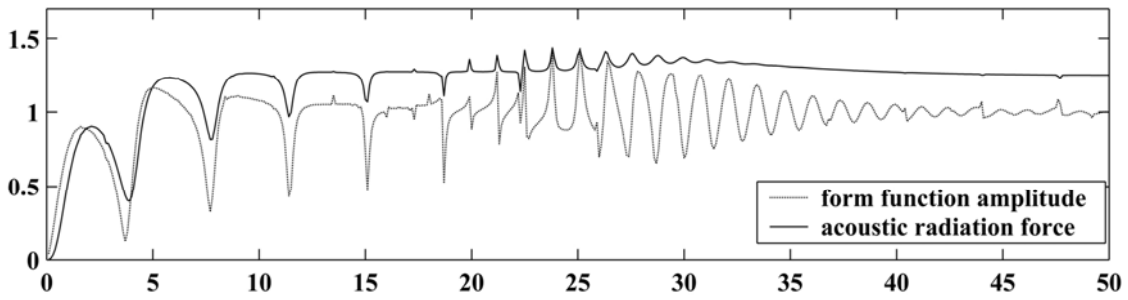


(a) $\bar{V}_F = 0.9$

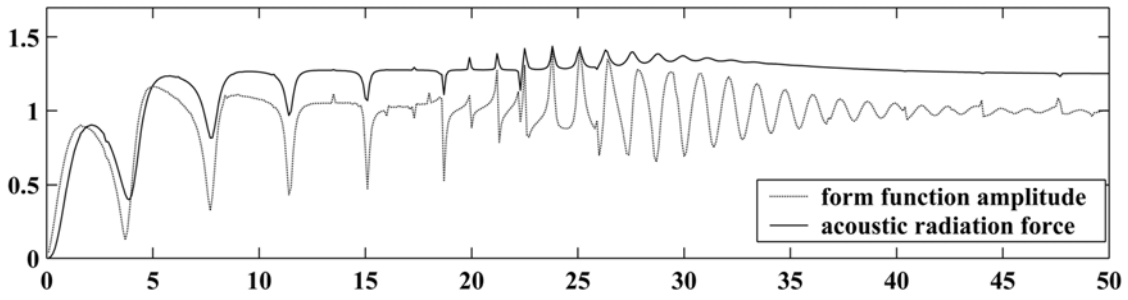


(b) $\bar{V}_F = 0.7$

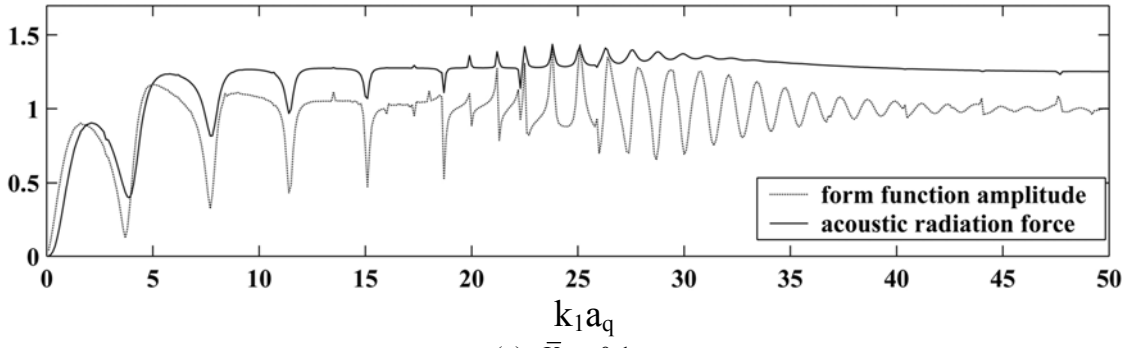
https://doi.org/10.1017/jmech.2011.27 Published online by Cambridge University Press



(c) $\bar{V}_F = 0.5$

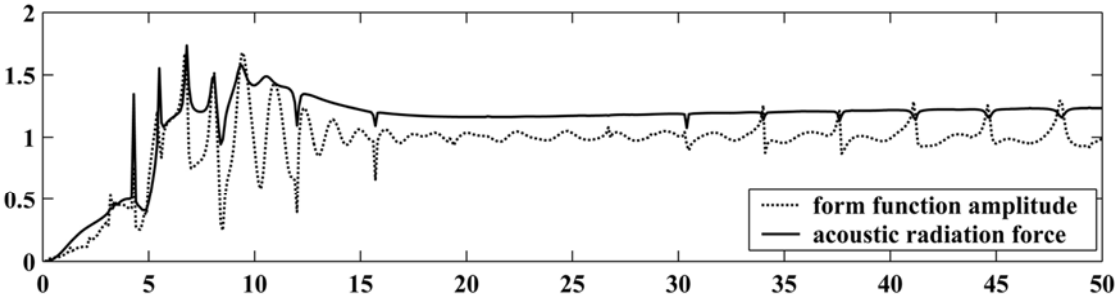


(d) $\bar{V}_F = 0.3$

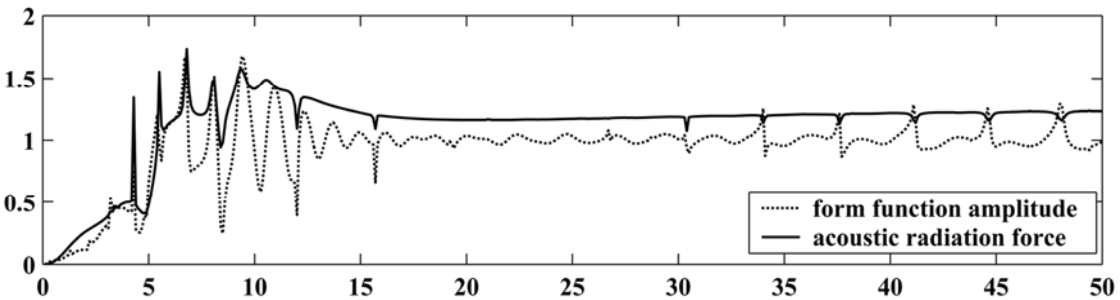


(e) $\bar{V}_F = 0.1$

Fig. 6 Variations of normalized backscattering form function amplitudes (dotted-line) and the radiation force function (solid line) with dimensionless frequency, for a $h/a_q = 0.04$ thickness functionally graded cylindrical shell

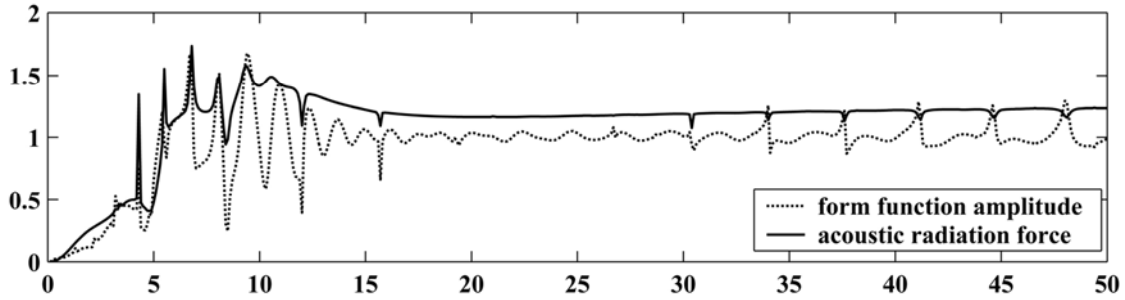


(a) $\bar{V}_F = 0.9$

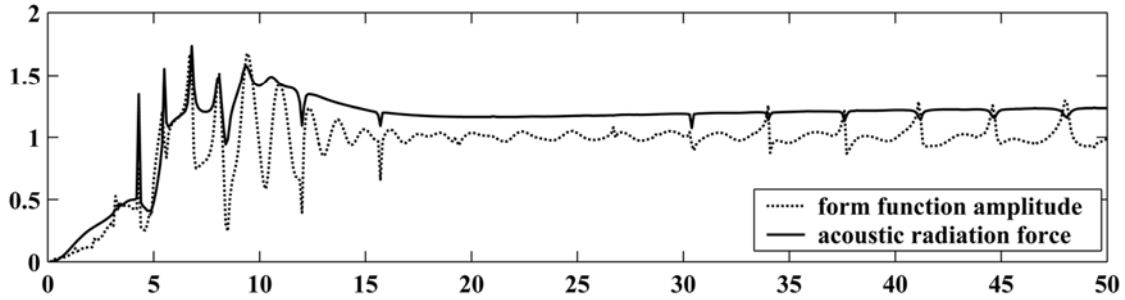


(b) $\bar{V}_F = 0.7$

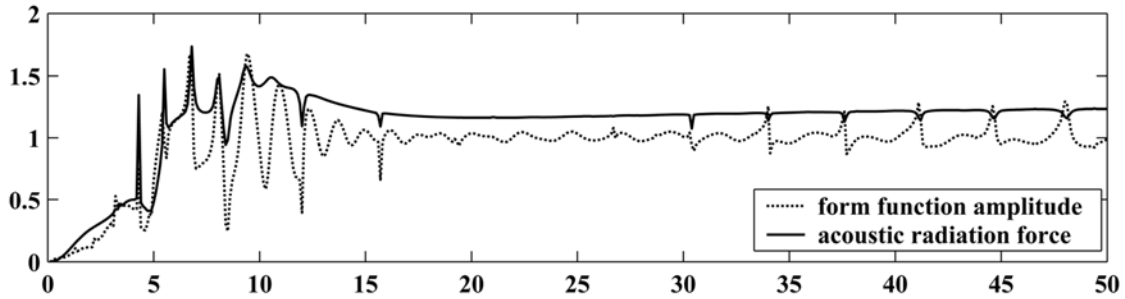
https://doi.org/10.1017/jmech.2011.27 Published online by Cambridge University Press



(c) $\overline{V}_F = 0.5$



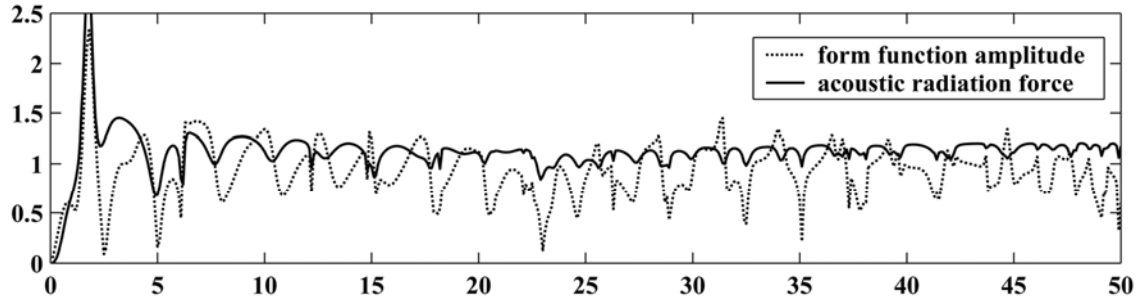
(d) $\overline{V}_F = 0.3$



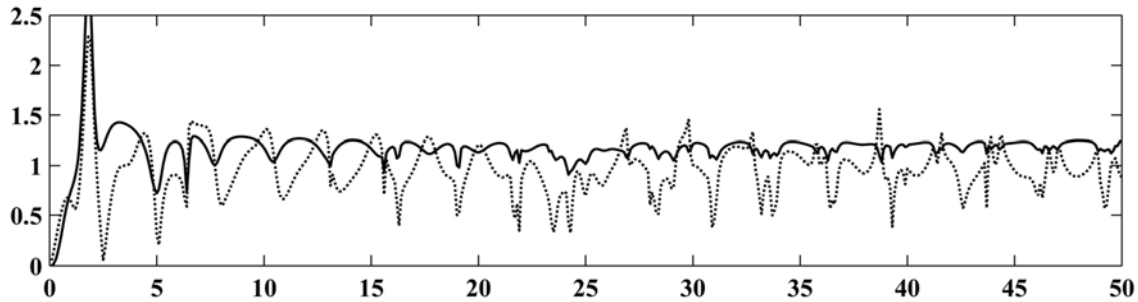
$k_1 a_q$

(e) $\overline{V}_F = 0.1$

Fig. 7 Variations of normalized backscattering form function amplitudes (dotted-line) and the radiation force function (solid line) with dimensionless frequency, for a $h/a_q = 0.1$ thickness functionally graded cylindrical shell

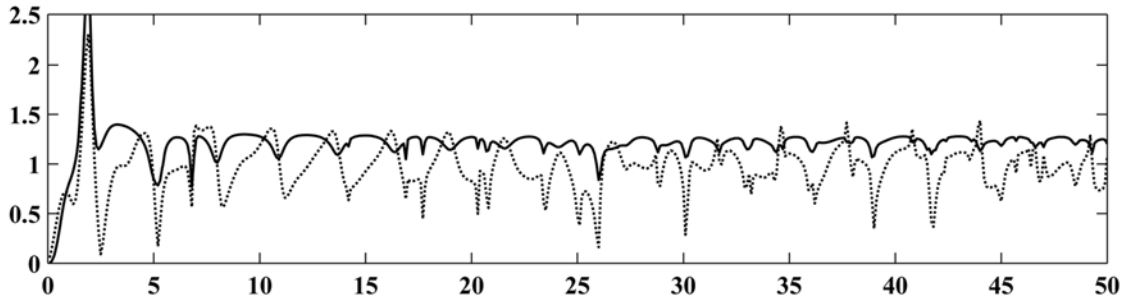


(a) $\overline{V}_F = 0.9$

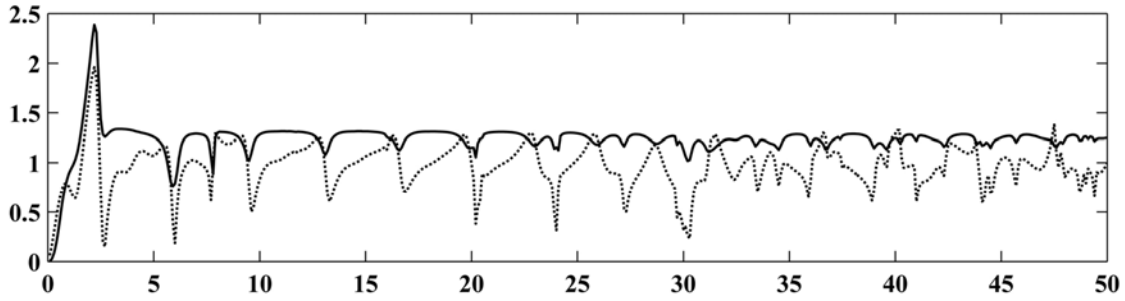


(b) $\overline{V}_F = 0.7$

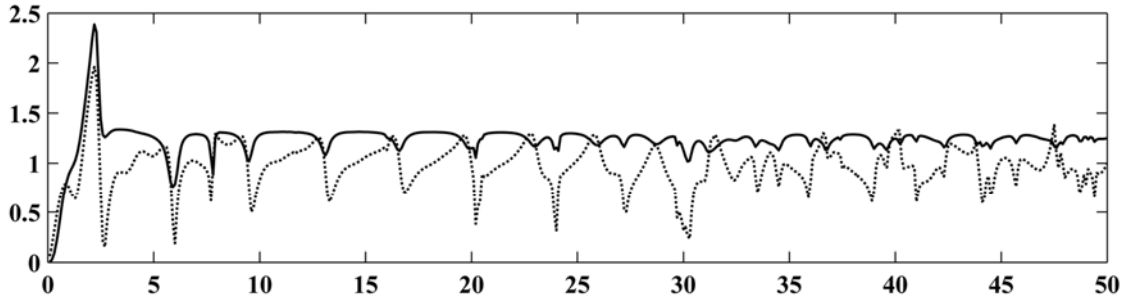
https://doi.org/10.1017/jmech.2011.27 Published online by Cambridge University Press



(c) $\overline{V}_F = 0.5$

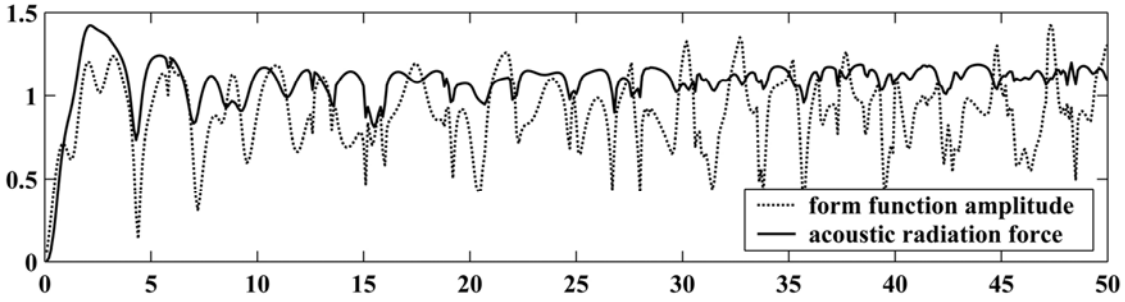


(d) $\overline{V}_F = 0.3$

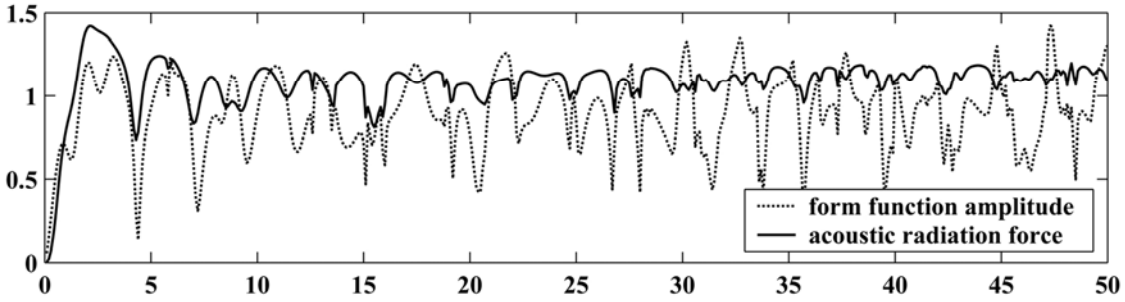


(e) $\overline{V}_F = 0.1$

Fig. 8 Variations of normalized backscattering form function amplitudes (dotted-line) and the radiation force function (solid line) with dimensionless frequency, for a $h/a_q = 0.5$ thickness functionally graded cylindrical shell



(a) $\overline{V}_F = 0.9$



(b) $\overline{V}_F = 0.7$

https://doi.org/10.1017/jmech.2011.27 Published online by Cambridge University Press

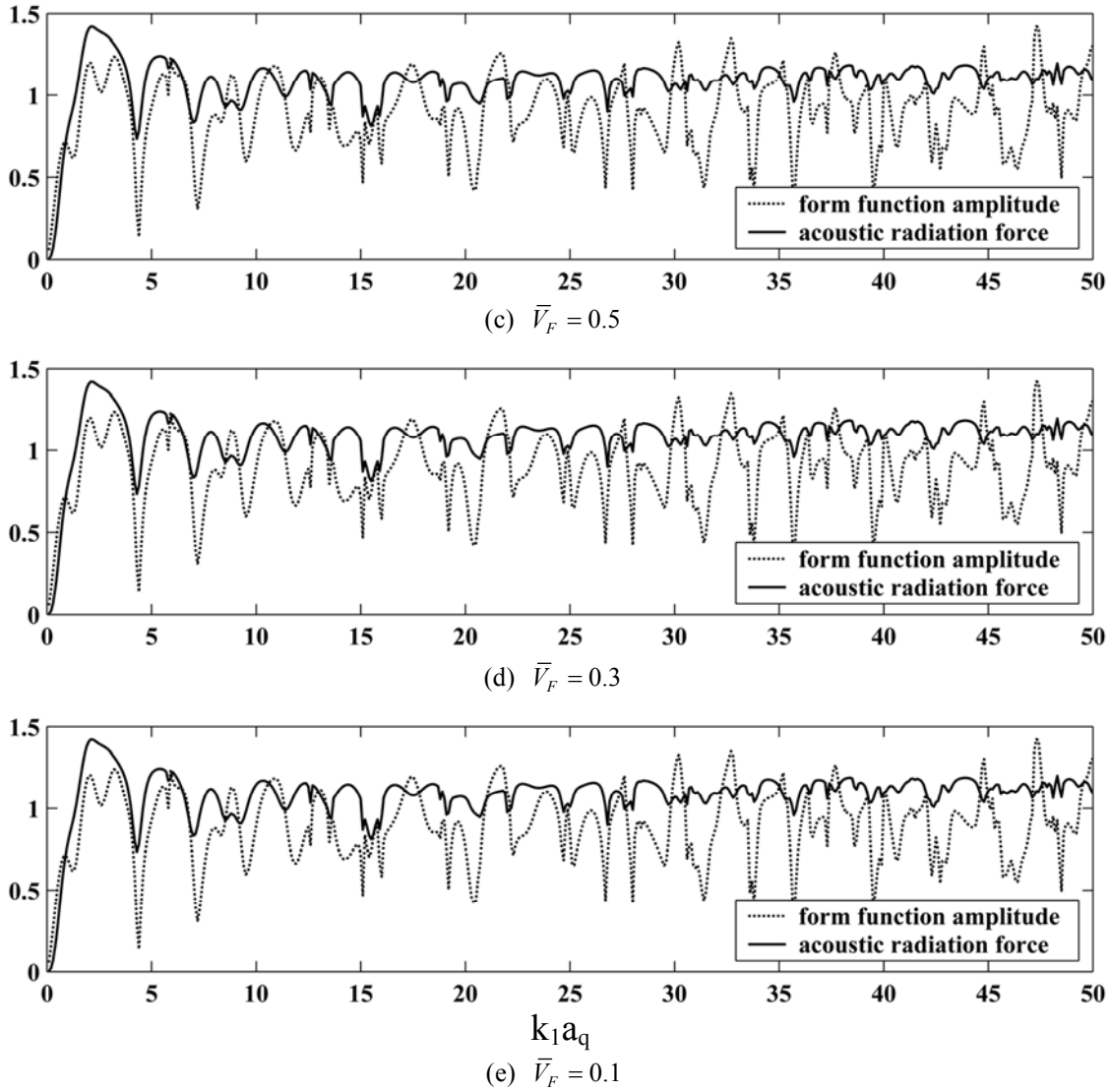


Fig. 9 Variations of normalized backscattering form function amplitudes (dotted-line) and the radiation force function (solid line) with dimensionless frequency, for a $h/a_q = 0.5$ thickness functionally graded cylindrical shell

From resonance acoustic spectroscopy (RAS), it is well-known that the resonance spectra (part) of form function amplitude superimposed on a smooth background spectra [13]. The background signal or the non-resonant part of scattered acoustic field is due to the overall rigidity of the structure which depends just on the geometry, size and density of the object. What is interesting is that this character is observed for the acoustic radiation force function, especially in the case of thin shells. But better examination of the form function spectra and the radiation force functions shows that the resonance frequencies are more visible in the form function curves in comparison to the radiation force functions. On one hand, it may be linked to this event that the contribution of the background signals in creating the radiation force functions are more than them superimposed on the form function amplitude spectra, especially in higher frequencies. On the other hand, considering this fact that the origin of the acoustic radiation force is the asymmetric pattern of the near-field scattered waves and their constructive-destructive interference with the incident field and also, mentioning the fluctuating behavior of these waves in the near-field zones, it may be inferred that the contribution of resonance response of the shell in comparison with the background part (*i.e.*, non-resonant or geometrical reflection) appeared in radiation force function is weakened. Additionally, as the frequency increases, the radiation force function converts to a smooth line (*i.e.*, analogous to the radiation force function of a rigid or soft cylinder in higher frequencies [28,30]).

Both the radiation force function and the form function amplitude (*i.e.*, resonance frequencies) of the FGM shell with different overall volume concentrations of constituents and different profile of variations, for all shell wall-thicknesses have different characteristics of wave propagation and radiation damping. Both the frequency and the quality (amplitude and band-width) of the resonances which are visible in these spectra vary with the change in the gradients fraction and the style of distribution. The frequency spectra of the radiation force and the form function of the graded shells are

https://doi.org/10.1017/jmech.2011.27 Published online by Cambridge University Press

nearly between those of the Al (*i.e.*, $\bar{V}_F = 1$) and ZrO_2 (*i.e.*, $\bar{V}_F = 0$) shells, in our interested range of frequency: the former is the low frequency bound and the latter the high frequency bound. As $\bar{V}_F$ changes from 0.1 to 0.9, the resonances of the graded shell vary from the resonances corresponding to the single ZrO_2 shell to the resonances of the single Al and a general left-ward shift is observed. Comparing the spectra of the thick graded shell in Figs. 8 and 9 with the thin ones in Figs. 6 and 7, clearly shows that in the case of thick shells, we have a more crowded region of resonances in comparison to the thin shells. This character may be helpful since many alternatives of resonance frequencies exist which can be taken in order to track and evaluate the properties of the graded shells.

Finally, to check overall validity of the work, we computed the normalized radiation force function amplitude, Y_p, with dimensionless frequency, $k_1 a_q$, for an air-filled single-layer Lucite shell submerged in water. For this, we set $q = 1$, $\gamma \to 0$ in Eq. (29), $h/a_q = 0.5$, $\rho_c^{(j)} = 1191\text{kg/m}^3$, $c_{11}^{(j)} = c_{22}^{(j)} = 8.61\text{GPa}$, $c_{12}^k = 4.34\text{GPa}$, $c_{33}^{(j)} = 2.13\text{GPa}$ where $j = 1, 2, \ldots, 100$, $\rho_1 = 1000\text{kg/m}^3$, $c_1 = 1500\text{m/s}$, $\rho_2 = 1.2\text{kg/m}^3$ and $c_2 = 340\text{m/s}$, in our general MATLAB code. The numerical results, as shown in Fig. 10(a) show good agreement with those displayed in Fig. 2(b) of [48]. As a further check, we computed the variations of the global scattering coefficient with dimensionless frequency for a two-layered air-filled aluminium (Al)-tungsten carbide (WC) 2%-thickness shell submerged in water by setting $h/a_q = 0.02$, $q = 2$, $\rho_c^1 = 2790\text{kg/m}^3$, $c_{11}^k = c_{22}^k = 113.5\text{GPa}$, $c_{12}^k = 59.9\text{GPa}$, $c_{33}^k = 26.8\text{GPa}$ $\rho_c^2 = 13800\text{kg/m}^3$, $c_{11}^k = c_{22}^k = 649.2\text{GPa}$, $c_{12}^k = 166.0\text{GPa}$, $c_{33}^k = 241.6\text{Gpa}$, $\lambda^{[2]} = 166.0\ \text{GPa}$, $\mu^{[2]} = 241.6\text{GPa}$, $\rho_1 = 1000\text{kg/m}^3$, $c_1 = 1480\text{m/s}$, $\rho_2 = 1.2\text{kg/m}^3$ and $c_2 = 340\text{m/s}$ in our general MATLAB code. The numerical results, as shown in Fig. 10(b) show good agreement with those displayed in Fig. 11 of [49]. Finally, we computed the variations of the global scattering coefficient, $|f_n|$, with dimensionless frequency, $k_1 a_q$, for an air-filled single-layer aluminium shell submerged in water. For this, we greatly increased the number of layers (*i.e.*, set $q = 100$) in an FGM cylindrical shell and let $\gamma \to 0$ ($V_F \to 1$) in Eq. (29) by setting $h/a_q = 0.8$, $q = 100$, $\rho_c^{(j)} = 2790\text{kg/m}^3$, $c_{11}^{(j)} = c_{22}^{(j)} = 113.1\text{GPa}$, $c_{33}^{(j)} = 26.7\text{GP}$, where $j = 1, 2, \ldots, 100$, $\rho_1 = 1000\text{kg/m}^3$, $c_1 = 1480\text{m/s}$, $\rho_2 = 1.2\text{kg/m}^3$ and $c_2 = 344\text{m/s}$, in our general MATLAB code. The numerical results, as shown in Fig. 10(c) show good agreement with those displayed in Fig. 1 of [50].

4. CONCLUSIONS

In this paper, we employ a laminate approximate model along with the so-called state space formulation in conjunction with the transfer matrix (T-matrix) approach to develop the theory of acoustic radiation force of isotropic homogeneous cylindrical shells (*i.e.*, Mitri's work) to the orthotropic functionally graded cylindrical shells. An elegant self-consistent micromechanical model which assumes an interconnected skeletal microstructure in the graded region is employed to represent the elastic properties of FGM interlayer. Particular attention is paid on comparing the dynamical response of these models in a wide range of frequency and for different shell wall-thicknesses. Also, computing the radiation force (*i.e.*, as a near-field quantity) for different profile of variation in FGM interlayer and various shell-wall thicknesses and comparing with the back-scattered form function amplitude (*i.e.*, as a far-field quantity) show that how this spectrum can be used for non-contact non-destructive evaluation of design characters of FGM shells (*i.e.*, the profile of material distribution and the overall volume concentration of constituting materials). The results show that how the dips and peaks appeared in the radiation force function can be interpreted as the resonances associated with the surface waves whirling around the shell which are appeared in the scattered acoustic field. Both the amplitude and the resonance frequencies (dips and peaks) in the radiation force function are the function of the composition of the FGM interlayer.

APPENDIX I

$$\mathbf{M}^k = \begin{bmatrix} \mathbf{M}_{11}^k & \mathbf{M}_{12}^k \\ \mathbf{M}_{21}^k & \mathbf{M}_{22}^k \end{bmatrix},$$

where

$$\mathbf{M}_{11}^k = \begin{bmatrix} \dfrac{1}{r} & -\dfrac{\partial}{r\partial\theta} \\ \dfrac{c_{12}^k}{c_{11}^k}\dfrac{\partial}{r\partial\theta} & -\dfrac{c_{12}^k}{c_{11}^k}\dfrac{1}{r} \end{bmatrix},$$

$$\mathbf{M}_{12}^k = \begin{bmatrix} 0 & \dfrac{1}{c_{33}^k} \\ \dfrac{1}{c_{11}^k} & 0 \end{bmatrix},$$

$$\mathbf{M}_{21}^k = \begin{bmatrix} -\dfrac{e^k}{r^2}\dfrac{\partial}{\partial\theta} & \left(\rho_c^k\dfrac{\partial^2}{\partial t^2} + \dfrac{e^k}{r^2}\right) \\ \left(\rho_c^k\dfrac{\partial^2}{\partial t^2} - c_{44}^k\dfrac{\partial^2}{\partial z^2} - \dfrac{e^k}{r^2}\dfrac{\partial^2}{\partial\theta^2}\right) & -\dfrac{e^k}{r^2}\dfrac{\partial}{\partial\theta} \end{bmatrix},$$

$$\mathbf{M}_{22}^k = \begin{bmatrix} \dfrac{1}{r}\left(\dfrac{c_{12}^k}{c_{11}^k} - 1\right) & -\dfrac{\partial}{r\partial\theta} \\ -\dfrac{c_{12}^k}{c_{11}^k}\dfrac{\partial}{r\partial\theta} & -\dfrac{2}{r} \end{bmatrix},$$

in which $e^k = c_{22}^k - \dfrac{(c_{12}^k)^2}{c_{11}^k}$.

https://doi.org/10.1017/jmech.2011.27 Published online by Cambridge University Press

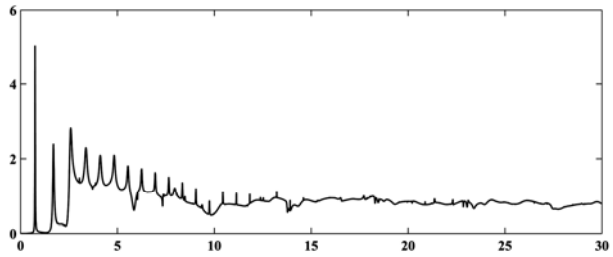


Fig. 10(a) Variations of the radiation force function with dimensionless frequency for an air-filled h/a_q = 0.5 thickness single-layer Lucite shell submerged in water (——— Mitri's results [48]; multilayered Aluminium shell)

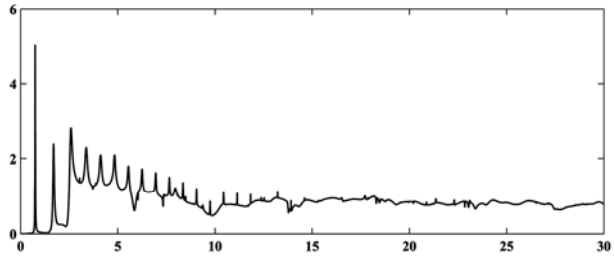


Fig. 10(b) Variations of the global scattering coefficient with dimensionless frequency for a two-layered air-filled aluminium (Al) - tungsten carbide (WC) 2%-thickness shell submerged in water for selected mode numbers n = 0, 1, 2, 3, 4 (——— Joo *et al's* results [49]; ∘ two layered Al/WC shell)

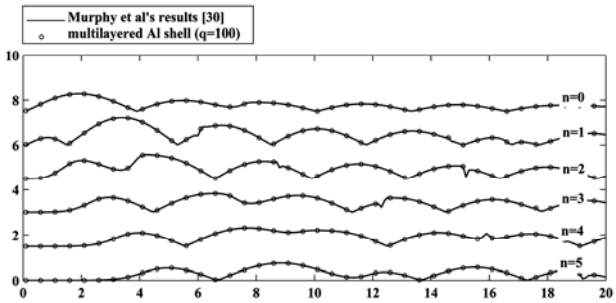


Fig. 10(c) Variations of the global scattering coefficient, with dimensionless frequency for an air-filled single-layer aluminium shell submerged in water (——— Murphy *et al* results [50]; ∘ multilayered Aluminium shell)

APPENDIX II

$$\mathbf{D}_n^k = \begin{bmatrix} \mathbf{D}_{11,n}^k & \mathbf{D}_{12,n}^k \\ \mathbf{D}_{21,n}^k & \mathbf{D}_{22,n}^k \end{bmatrix},$$

where

$$\mathbf{D}_{11}^k = \begin{bmatrix} \frac{1}{\xi} & \frac{n}{\xi} \\ \frac{c_{12}^k}{c_{11}^k}\frac{n}{\xi} & -\frac{c_{12}^k}{c_{11}^k}\frac{1}{\xi} \end{bmatrix},$$

$$\mathbf{D}_{12}^k = \begin{bmatrix} 0 & 1 \\ \frac{c_{33}^k}{c_{11}^k} & 0 \end{bmatrix},$$

$$\mathbf{D}_{21}^k = \begin{bmatrix} -\frac{e^k}{c_{33}^k}\frac{n}{\xi^2} & \frac{1}{c_{33}^k}\left(-\rho_c^k\omega^2 a_q^2 + \frac{e^k}{\xi^2}\right) \\ \frac{1}{c_{33}^k}\left(-\rho_c^k\omega^2 a_q^2 + \frac{e^k n^2}{\xi^2}\right) & \frac{e^k}{c_{33}^k}\frac{n}{\xi^2} \end{bmatrix},$$

$$\mathbf{D}_{22}^k = \begin{bmatrix} \frac{1}{\xi}\left(\frac{c_{12}^k}{c_{11}^k} - 1\right) & -\frac{n}{\xi} \\ \frac{c_{12}^k}{c_{11}^k}\frac{n}{\xi} & -\frac{2}{\xi} \end{bmatrix},$$

REFERENCES

1. Yamanouchi, M., Koizumi, M., Hirai, T. and Shiota, I., *Proceedings of the First International Symposium on Functionally Gradient Materials*, Sendai, Japan (1990).
2. Holt, J. B., Koizumi, M., Hirai, T. and Munir, Z. A., *Ceramic Transaction: Functionally Gradient Materials*, **34**, Ohio, Westerville, The American Ceramic Society (1993).
3. Koizumi, M., The Concept of FGM, in J.B. Holt, M. Koizumi, T. Hirai, Z. A. Munir Eds., *Ceramic Transaction: Functionally Gradient Materials*, **34**, Ohio, Westerville, The American Ceramic Society, pp. 3–10 (1993).
4. Suresh, S. and Mortensen, A., *Fundamentals of Functionally Graded Materials*, IOM Communications, London (1998).
5. Miyamoto, Y., Kaysser, W. A., Rabin, B. H., Kawasaki, A. and Ford, R. G., *Functionally Graded Materials: Design, Processing and Applications*, Chapman Hall (1999).
6. Talmant, M. and Batard, H., "Material Characterization and Resonant Scattering by Cylinders," *Proceedings of the IEEE Ultrasonics Symposium,* **3**, pp. 1371–1380 (1994).
7. Migliori, A. and Sarrao, J. L., "Resonant Ultrasound Spectroscopy: Applications to Physics," *Materials Measurements and Nondestructive Evaluation*, Wiley, New York (1997).
8. Tesei, A., Fox, W. L. J., Maguer, A. and Lovik, A., "Target Parameter Estimation Using Resonance Scattering Analysis Applied to Air-Filled, Cylindrical Shells in Water," *Journal of the Acoustical Society of America*, **108**, pp. 2891–2910 (2000).
9. Guicking, D., Goerk, K. and Peine, H., "Recent Advances in Sonar Target Classification," *Proceedings of SPIE*, *International Society for Optical Engineer-*

https://doi.org/10.1017/jmech.2011.27 Published online by Cambridge University Press

ing, 1700, pp. 2–15 (1992).
10. Honarvar, F. and Sinclair, A. N., "Nondestructive Evaluation of Cylindrical Components by Resonance Acoustic Spectroscopy," *Ultrasonic*, **36**, pp. 845–854 (1998).
11. Gaunaurd, G. C., "Elastic and Acoustic Resonance Wave Scattering," *Applied Mechanical Review*, **42**, pp. 143–192 (1989).
12. Uberall, H., *Acoustic Resonance Scattering, Gordon and Breach Science*, Philadelphia (1992).
13. Veksler, N. D., *Resonance Acoustic Spectroscopy, Springer Series on Wave Phenomena,* Springer-Verlag, Berlin (1993).
14. Honarvar, F. and Sinclair, A. N., "Acoustic Wave Scattering from Transversely Isotropic Cylinders," *Journal of the Acoustical Society of America,* **100**, pp. 57–63 (1996).
15. Hasheminejad, S. M. and Rajabi, M., "Acoustic Scattering Characteristics of Thick-Walled Orthotropic Cylindrical Shell at Oblique Incidence," *Ultrasonics*, **47**, pp. 32–48 (2007).
16. Hasheminejad, S. M. and Rajabi, M., "Acoustic Resonance Scattering from a Submerged Functionally Graded Cylindrical Shell," *Journal of Sound and Vibration*, **302**, pp. 208–228 (2007).
17. Rajabi, M. and Hasheminejad, S. M., "Acoustic Resonance Scattering from a Multilayered Cylindrical Shell with Imperfect Bonding," *Ultrasonics,* (2009).
18. Lee, C. P. and Wang, T. G., "Acoustic Radiation Pressure," *Journal of the Acoustical Society of America*, **94**, pp. 1099–1109 (1993).
19. Nightingale, K., Soo, M. S., Nightingalo, R. and Trahey, G., "Acoustic Radiation Force Impulse Imaging: In Vivo Demonstration of Clinical Feasibility," *Ultrasonic Medical Biology*, **28**, pp. 227–235 (2002).
20. Sarvazyan, R. P., Rudenko, O. V., Swanson, S. D., Fowlkes, J. B. and Emelianov, S. Y., "Shear Wave Elasticity Imaging: A New Ultrasonic Technology of Medical Diagnostics," *Ultrasonic Medical Biology,* **24**, pp. 1419–1435 (1998).
21. Fatemi, M. and Greenleaf, J. F., "Ultrasound Stimulated Vibro-Acoustic Spectroscopy," *Science*, **280**, pp. 82–85 (1998).
22. Fatemi, M. and Greenleaf, J. F., "Vibro-Acoustography: An Imaging Modality Based on Ultrasound-Stimulated Acoustic Emission," *Natural Academic of Science of USA*, **96**, pp. 6603–6608 (1999).
23. Dunn, F., Averbach, A. J. and O'Brein, D. J., "A Primary Method for the Determination of Ultrasonic Intensity with the Elastic Sphere Radiometer," *Acustica*, **38**, pp. 58–61 (1977).
24. Rayleigh, R. W. S., *On the Pressure of Vibrations, Philosophical Magazine,* **3**, pp. 338–346 (1902).
25. Awatani, J., "Study on Acoustic Radiation Pressure (IV), Radiation Pressure on a Cylinder," *Memoirs of the Institute of Scientific and Industrial Research*, Osaka University, **12**, pp. 95–102 (1955).
26. Zhuk, A. P., "Radiation Force Acting on a Cylindrical Particle in a Sound Field," *International Applied Mechanics*, **22**, pp. 689–693 (1986).
27. Hasegawa, T., Saka, K., Inoue, N. and Matsuzawa, K., "Acoustic Radiation Force Experienced by a Solid Elastic Cylinder in a Plane Progressive Sound Field," *Journal of the Acoustical Society of America*, **83**, pp. 1770–1775 (1988).
28. Hasegawa, T., Hino, Y., Annou, A., Noda, H. and Kato, M., "Acoustic Radiation Pressure Acting on Spherical and Cylindrical Shells," *Journal of the Acoustical Society of America*, **93**, pp. 154–161 (1993).
29. Mitri, F. G., "Radiation Force Acting on an Absorbing Cylinder Placed in an Incident Plane-Progressive Acoustic Field," *Journal of Sound and Vibration*, **284**, pp. 494–502 (2005).
30. Mitri, F. G., "Theoretical Calculation of the Acoustic Radiation Force Acting on Elastic and Viscoelastic Cylinders Placed in a Plane Standing or Quasistanding Wave Field," *European Physical Journal B*, **44**, pp. 71–78 (2005).
31. Mitri, F. G., "Theoretical and Experimental Determination of the Acoustic Radiation Force Acting on an Elastic Cylinder in a Plane Progressive Wave-Far-Field Derivation Approach," *New Journal of Physics*, **8**, p. 138 (2006).
32. Pierce, A. D., "Acoustics; An Introduction to its Physical Principles and Applications," *American Institute of Physics*, New York (1991).
33. Chen, W. Q., Bian, Z. G. and Ding, H. J., "Three Dimensional Vibration Analysis of Fluid Filled Orthotropic FGM Cylindrical Shells," *International Journal of Mechanical Science*, **46**, pp. 159–171 (2004).
34. Nayfeh, A. H. and Nagy, P. B., "General Study of Axisymmetric Waves in Layered Anisotropic Fibers and Their Composites," *Journal of the Acoustical Society of America*, **99**, pp. 931–941 (1996).
35. Achenbach, J. D., *Wave Propagation in Elastic Solids*, North-Holland, New York (1976).
36. Musgrave, M. J. P., *Crystal Acoustics*, Holden-Day Series in Mathematical Physics (1970).
37. Shuvalov, A. L., "A Sextic Formalism for Three-Dimensional Elasto-Dynamics of Cylindrically Anisotropic Radially Inhomogeneous Materials," *Proceeding of Royal Society of London*, **459**, pp. 1611–1639 (2003).
38. Chang, H. H. and Tarn, J. Q., "A State Space Approach for Exact Analysis of Composite Laminates and Functionally Graded Materials," *International Journal of Solids and Structures,* **44**, pp. 1409–1422 (2007).
39. Lee, W. M. and Chen, J. T., "Scattering of Flexural Wave in Thin Plate with Multiple Circular Holes by Using the Multipole Trefttz Method," *International Journal of Solids and Structures*, **47**, pp. 1118–1129 (2010).
40. Gantmakher, F. R., *The Theory of Matrices,* New York, Chelsea (1959).
41. Pease, M. C., *Methods of Matrix Algebra*, Academic (1965).
42. Chen, W. Q. and Ding, H. J., "Free Vibration of

https://doi.org/10.1017/jmech.2011.27 Published online by Cambridge University Press

Multi-Layered Spherically Isotropic Hollow Spheres," *International Journal of Mechanical Science,* **43**, pp. 667–680 (2001).
43. Chen, J. T., Chen, C. T., Chen, P. Y. and Chen, I. L., "A Semi-Analytical Approach for Radiation and Scattering Problems with Circular Boundaries," *Computational Methods and Applications in Mechanical Engineering*, **196**, pp. 2751–2764 (2007).
44. Hill, R., "A Self-Consistent Mechanics of Composite Materials," *Journal of Mechanics and Physics of Solids*, **13**, pp. 213–222 (1965).
45. Reiter, T., Dvorak, G. J. and Tvergaard, V., "Micromechanical Models for Graded Composite Materials," *Journal of Mechanics and Physics of Solids*, **45**, pp. 1281–1302 (1997).
46. Lee, W. M. and Chen, J. T., "Scattering of Flexural Wave in Thin Plate with Multiple Inclusions by Using Null-Field Integral Equation Approach," *Journal of Sound and Vibration*, **329**, pp. 1042–1061 (2010).
47. Yosioka, K. and Kawasima, Y., "Acoustic Radiation Pressure on a Compressible Sphere," *Acustica*, **5**, pp. 167–173 (1955).
48. Mitri, F. G., "Frequency Dependence of the Acoustic Radiation Force Acting on Absorbing Cylindrical Shells," *Ultrasonics,* **43**, pp. 271–277 (2005).
49. Joo, Y. S., Ih, J. G. and Choi, M. S., "Inherent Background Coefficients for Acoustic Resonance Scattering from Submerged, Multilayered, Cylindrical Structures," *Journal of the Acoustical Society of America*, **103**, pp. 900–910 (1998).
50. Murphy, J. D., Breitenbach, E. D. and Uberall, H., "Resonance Scattering of Acoustic Waves from Cylindrical Shells," *Journal of the Acoustical Society of America*, **64**, pp. 677–683 (1978).

(Manuscript received March 3, 2010,
accepted for publication May 26, 2010.)

https://doi.org/10.1017/jmech.2011.27 Published online by Cambridge University Press